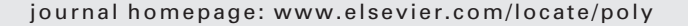


Contents lists available at SciVerse ScienceDirect

Polyhedron





EPR studies of a cyano-bridged $\{Fe_2^{III}Ni^{II}\}$ coordination complex and its corresponding Fe^{III} mononuclear building-block

Christopher C. Beedle a, Yuan-Zhu Zhang b, Stephen M. Holmes c,*, Stephen Hill a,d,*

- ^a National High Magnetic Field Laboratory, Florida State University, Tallahassee, FL 32310, USA
- ^b Department of Chemistry & Biochemistry, University of Missouri St. Louis, St. Louis, MO 63121, USA
- ^c Center of Nanoscience, University of Missouri St. Louis, St. Louis, MO, 63121, USA
- ^d Department of Physics, Florida State University, Tallahassee, FL 32306, USA

ARTICLE INFO

Article history: Received 8 January 2013 Accepted 11 April 2013 Available online 18 April 2013

Keywords:
High-field electron paramagnetic resonance
(HF-EPR)
Low-spin Fe^{III}
Single-molecule magnet (SMM)
Tris-pyrazoylborate
Cyano-bridged coordination complex
Magnetoanisotropy

ABSTRACT

High-field/frequency electron paramagnetic resonance measurements have been performed on a cyanobridged trinuclear Fe^{III}Ni^{II} complex and an analogous mononuclear Fe^{III} building block. The mononuclear Fe^{III} complex exhibits a low-spin configuration resulting from a strong-field coordination environment and can be modeled as an effective s = 1/2 Kramers ion that exhibits significant g-anisotropy: $g_z = 3.7$, $g_y = 2.2$ and $g_x = 1.92$. The corresponding Fe₂^{III}Ni^{II} complex possesses an S = 2 spin ground state as a result of ferromagnetic exchange that is mediated by the bridging cyano ligands. Simulations of frequency dependent EPR data establish that the Fe₂^{III}Ni^{II} complex exhibits easy-axis type magnetoanisotropy, with best-fit simulation parameters of: S = 2, D = -2.09 cm⁻¹, E = 0.08 cm⁻¹, $B_4^{\ 0} = 2.3 \times 10^{-3}$ cm⁻¹, $g_z = 2.4$, $g_y = g_x = 1.95$.

© 2013 Elsevier Ltd. All rights reserved.

1. Introduction

There is currently much interest in studying magnetic systems where the magnetic properties of molecular building-blocks can be examined independently and the results used to analyze more complicated polynuclear clusters [1–5]. Furthermore, molecular magnetic complexes that incorporate Fe^{III} ions are of interest because they have been shown to exhibit spin-crossover behavior [6,7], and the ligand-field strength of coordinated peripheral ligands can dictate whether the exhibited ground state is in a low-spin (s = 1/2 doublet) or high-spin (s = 5/2 sextet) configuration.

In recent years a systematic approach has been developed to synthesize mononuclear cyanoferrate building blocks that can be subsequently used to synthesize polynuclear systems with intriguing magnetic properties [4,5,8,9]. It has been shown that the electronic properties of these systems can be readily tuned through systematic modification of ancillary ligands [4,5,9].

In this study high-field/frequency oriented single-crystal and powder EPR techniques were employed to study the tricyanoferrate(III) building block [NEt₄][(Tp*Me)Fe^{III}(CN)₃]·2H₂O (**1**) [5] and the trinuclear complex [{(Tp*Me)Fe(CN)₃}₂Ni(DETA)(H₂O)]·6H₂-O·CH₃CN (**2**).

2. Experimental

[NEt₄][(Tp*^{Me})Fe^{III}(CN)₃]·2H₂O (1) [5] crystallizes in the space group P21/n with Z'=1. The octahedrally coordinated Fe^{III} ion is capped by a tridentate Tp*^{Me} (Tp*^{Me} = tris(3,4,5-trimethylpyrazole)borate) ligand and the coordination sphere is completed by three CN⁻¹ ligands that are coordinated in an Fe–CN fashion (strong-field environment).

 $\{[(Tp^{*Me})Fe^{III}(CN)_3]_2[Ni^{II}(DETA)(OH_2)]\}\cdot 6H_2O\cdot MeCN$ (2) crystallizes in the space group PI with a single molecule in the asymmetric unit. The octahedrally coordinated central Ni^{II} ion is capped by a tridentate DETA ligand (diethylenetriamine) and a single water molecule. The Ni^{II} is coupled to the peripheral Fe^{III} units via two bridging CN^{-1} ligands that are arranged in $Fe^{-CN-Ni-NC-Fe}$ mode to form the exchange-coupled magnetic core.

High-field powder EPR data were collected at the US National High Magnetic Field Laboratory Electron Magnetic Resonance facility using a transmission probe in which microwaves are propagated through cylindrical light-pipes. High-frequency microwaves were generated by a phase-locked Virginia Diodes solid-state source operating at 13 ± 1 GHz, followed by a chain of multipliers and amplifiers. High magnetic fields were provided by a $17 \, \mathrm{T}$ superconducting magnet [10].

Single-crystal high-field/frequency EPR experiments were performed in a Quantum Design PPMS system equipped with a 7 T

^{*} Corresponding authors. Tel.: +1 8506441315 (S.M. Holmes). *E-mail addresses*: holmesst@umsl.edu (S.M. Holmes), shill@magnet.fsu.edu

superconducting magnet. A Millimeter-wave Vector Network Analyzer (MVNA) served as a microwave source and detector [11,12].

3. Data and discussion

Frequency dependent powder EPR data for 1, collected between 50 and 217 GHz at 5 K, are presented in Fig. 1. The spectra reveal three resonance branches (open black-squares, red-circles, and blue-diamonds) that intersect the origin in the frequency versus field plot (Fig. 1), and are assigned as the z, y and x intra-Kramers components of the ground state doublet. A fourth resonance was also observed that is consistent with an impurity phase with g = 2 (i.e. a slope of 28 GHz/T as $B \rightarrow 0$, see inset in Fig. 1) and was not featured in the EPR analysis for complex 1 analysis (isotropic impurities are commonly observed in EPR studies of transition metal complexes). The frequency dependent data were simulated (solid lines) assuming an effective s = 1/2 ground state, yielding an anisotropic g-tensor with values of $g_z = 3.7$ and $g_v = g_x = 2.2$. We note that a low-spin Fe^{III} (d^5) ion in an octahedral ligand environment will possess an orbitally degenerate ground state, thus explaining the observed anisotropy.

Single-crystal angle-dependent EPR data for complex **2** (Fe₂^{III-}Ni^{II}) are shown in Fig. 2. The data were collected at 236.6 GHz and 2 K. The spectra are dominated by a single broad peak at low applied fields (black arrow, θ = 0 in Fig. 2) and two broad features at higher fields (red and green arrows, respectively). We note that the hard-plane (B/|xy) ground state and excited state transitions lie out of the applied field range at 236.6 GHz (see Fig. 2, θ = 90 and θ = -90 angle positions), thus, angle-dependent hard-plane spectra for complex **2** were collected at 191 GHz (not shown).

Fig. 3 presents temperature dependent EPR data for complex **2** with the field aligned near the easy-axis (z-axis, θ = 0 angle position in Fig. 2). The data were collected at temperatures between 2 and 12.5 K at 326.6 GHz. The resonance observed at low fields (black arrow in Fig. 3) persists to the lowest measured temperature, and increases in intensity with decreasing temperature, which indicates that it originates from the lowest-lying sub-level

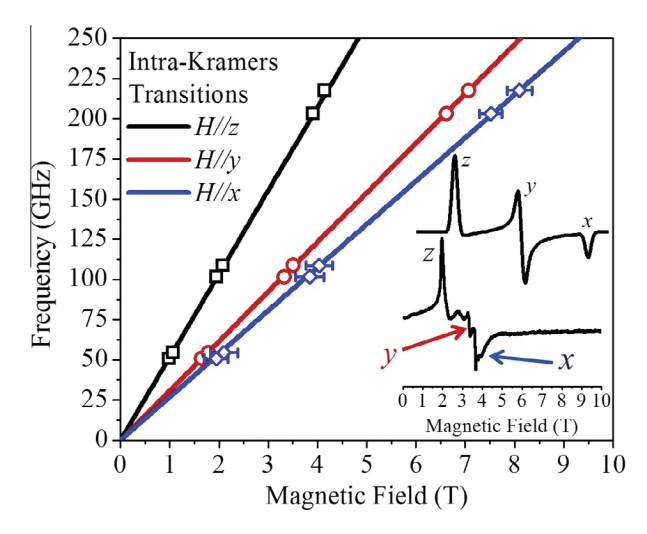


Fig. 1. The main panel shows frequency vs. field powder EPR data for complex **1** (Fe^{III} monomer) collected between 50 and 217 GHz at 5 K. The three resonance branches (open black-squares, red-circles and blue-triangles) are the experimental data for the three principal (x, y and z) g-values associated with the effective s = 1/2 ground state Kramers doublet. The solid lines were simulated with the Hamiltonian given in equation **1**, yielding the parameters: $g_z = 3.7$, $g_y = 2.2$ and $g_x = 1.92$. Inset (top) shows a simulated powder spectrum in derivative mode for a typical biaxial system and illustrates the line-shapes expected for the x, y and z components of the g-tensor. Inset (bottom) shows a representative powder EPR spectrum for complex **1** collected at 101.6 GHz. (Color online.)

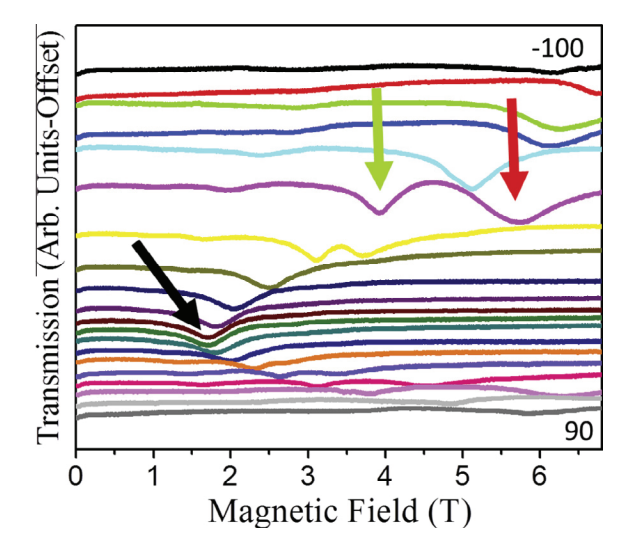


Fig. 2. Plot of angle-dependent single-crystal EPR data is presented and was collected at 236.6 GHz at 2 K for complex **2** (Fe₂^{III}Ni^{II}) in 10° steps. The black arrow denotes the angle position where the applied field is near the molecular *z*-axis (easy-axis, θ = 0), while the red and green arrows show transitions associated with the hard plane (see text for explanation). (Color online.)

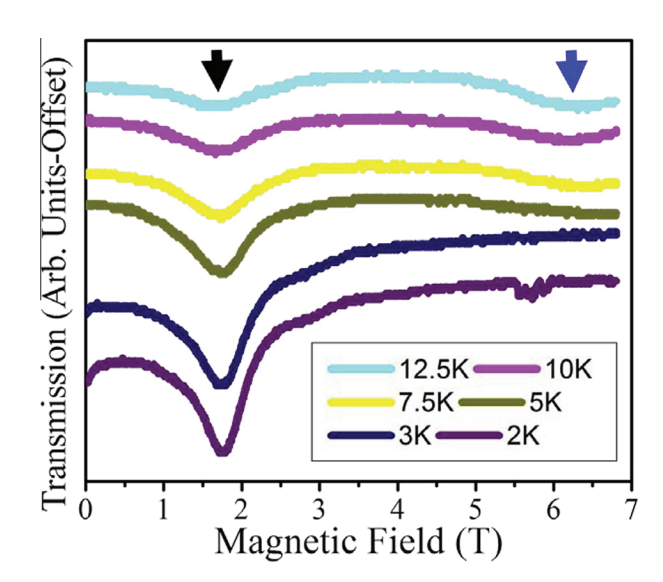


Fig. 3. Plot of temperature dependent single-crystal EPR data for complex **2** (Fe₂^{III}Ni^{II}) collected at 236.6 GHz, between 2 K and 12.5 K, with the field aligned near the *z*-axis (easy-axis). The black and blue arrows show the field positions of the *z*-axis ground state (GS) and first excited state (ES) resonances, respectively. (Color online.)

within the ground state spin-multiplet. At temperatures above 5 K a broad feature (blue arrow in Fig. 3) is clearly evident that is consistent with an excited state transition within the ground state spin-multiplet (*vide infra*). Temperature dependent studies (not shown) on the two resonances observed at higher magnetic fields (red and green arrows in Fig. 2) reveal that these transitions also persist to the lowest experimental temperatures and thus also originate from or within the ground state spin-multiplet. Note: the data for the high field peaks were collected at 191 GHz at the $\theta = -90$ angle position (B/|xy) shown in Fig. 3.

In order to gauge the spin ground state of complex **2**, and to deduce the magnitude and sign of the zero-field splitting parameter D, multi-frequency EPR studies were performed. A plot of frequency versus field is given in Fig. 4a for complex **2** and the experimental data (open squares, B/|z, and open circles, B/|xy) were

simulated (solid lines) employing the following effective spin Hamiltonian (1):

$$\hat{H} = \mu_{\rm B} \mathbf{B} \cdot \stackrel{\leftrightarrow}{\mathbf{g}} \cdot \hat{\mathbf{S}} + D\hat{\mathbf{S}}_{2}^{2} + E(\hat{\mathbf{S}}_{2}^{2} - \hat{\mathbf{S}}_{2}^{2}) + B_{A}^{0} \hat{\mathbf{0}}_{A}^{0}$$
(1)

Here, μ_B is the Bohr magneton, B is the applied magnetic field, g is the Landé g-tensor, \hat{S} is the spin-operator, D is the second-order axial zero-field splitting parameter, E is the second-order rhombic zero-field splitting parameter, and the last term is the axial fourth-order zero-field splitting term [13,14]. The best fit simulation parameters yielded values of: S=2, $D=-2.09~{\rm cm}^{-1}$, $E=0.08~{\rm cm}^{-1}$, $B_q^0=-2.3\times 10^{-3}~{\rm cm}^{-1}$, $g_z=2.4$, $g_y=g_x=1.95$ (a field misalignment of $\theta=20^\circ$ was included in the B//z (easy-axis) simulations (black and blue solid lines in Fig. 4a), as one cannot guarantee exact field alignment with the magnetic z-axis in a single-axis rotation EPR experiment.

First we comment on the assignment of an S = 2 ground state. As we have demonstrated, the Fe^{III} monomer building block (complex 1) can be treated as an effective s = 1/2 system, so from a simplistic structural point of view, coupling between the peripheral Fe^{III} building blocks and the central s = 1 Ni^{II} ion to form the corresponding Fe2 III Ni II trinuclear complex (complex 2) should result in either an antiferromagnetic S = 0 (S = 1/2 + 1/2 - 1 = 0) or a ferromagnetic S = 2 (S = 1/2 + 1/2 + 1 = 2) magnetic ground state. We have labeled and assigned the four main observed resonance branches for complex 1 in Fig. 4a, and these branches can be divided into two groups. With the field applied near the z-quantization axis, two resonance branches are observed and are assigned as the ground state (GS, black open circles) and the first exited state (ES, blue open square). Indeed, the excited state transition was only observed at 236.6 GHz at the frequencies and temperatures examined in these experiments; however, a feature is clearly evident in the temperature dependent studies (Fig. 3, blue arrow) that is both reproducible, and consistent with an excited state transition within the ground state spin-multiplet. When the field is then oriented in the hard-plane (B/|xy), again we observe two resonance branches that correspond to the ground state (GS) transition (red open circles) and an excited state (ES) transition (green open circles). The solid magenta triangles in Fig. 4a result from an isotropic paramagnetic impurity with a slope (solid magenta line) of g = 2(vide supra) and are thus not included in the main EPR. Zeeman diagrams for B/|z (easy-axis) and B/|xy (hard-plane) are presented in Fig. 4a and b, respectively. The observed transitions (represented by vertical lines) in Fig. 4a and b are color coded and correlate to the experimental data presented in Fig. 4a (the color coding scheme is uniform throughout Figs. 2-4, for complex 2). The resonance branches observed experimentally correlate very well to ground state and excited state transitions within the corresponding Zeeman diagrams, and further suggest that the assignment of the observed experimental resonance branches, and of a spin ground state of S = 2 is wholly consistent.

Attention is now turned to the sign and magnitude of the zero-field splitting (ZFS) in complex **2**. This system exhibits appreciable ZFS as indicated by the zero-field intercept (\sim 180 GHz) of the ground state B//z transition (black line in Fig. 4a), and it constrains the magnitude of D, while the slope of this resonance branch governs the value of g_z . Moreover, simulations for complex **2** yielded a negative axial zero-field splitting parameter D (D < 0), signifying the presence of easy-axis type magnetoanisotropy. The inclusion of a fourth-order axial zero-field splitting parameter (B_4^0) in the EPR simulations, in conjunction with a field misalignment of θ = 20°, was critical to account for the spacing between the ground state resonance branch and the excited state branch (open blue square and solid blue line). In addition, the value of g_{xy} and the rhombic E-term are constrained by the slope and spacing between the ground state and excited state resonance branches where B//xy

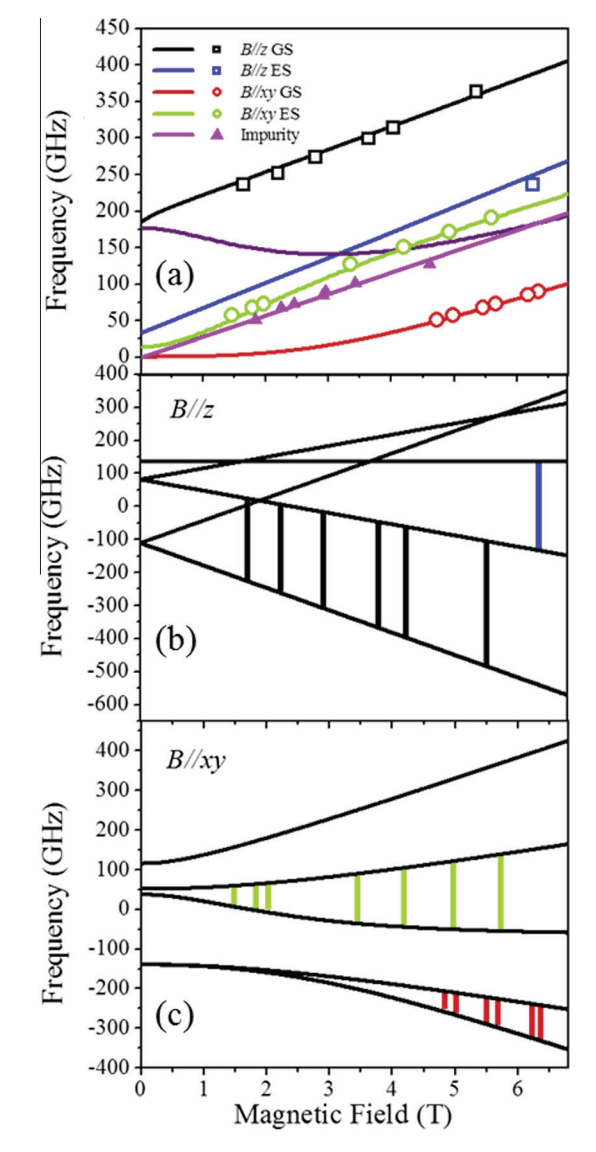


Fig. 4. Top panel (a) shows frequency-dependent EPR peak positions (open squares and open circles) for complex **2** (Fe₂^{III}Ni^{II}) plotted as a function of the applied magnetic field strength. The solid curves (see inset for color scheme assignments) correspond to simulations employing the Hamiltonian in Eq. (1). The magenta triangles and solid line represent an impurity phase with g = 2. (b and c) Zeeman energy diagrams are presented with B/|z and B/|xy, respectively. The positions of the EPR resonances (vertical lines) correlate to the observed experimental resonance positions (same color scheme as presented in a). (Color online.)

(red and green open circles and simulation lines, respectively). Finally, the value of $g_z = 2.4$ deduced through simulations is quite reasonable for a complex containing a Ni^{II} ion, though one would expect g-values greater than g = 2 for g_{xy} for such a compound. The smaller value of g_{xy} 1.95 extracted through EPR simulations most likely originates from the highly anisotropic low-spin Fe^{III} centers. In all, the EPR data presented here agree well with previously reported magnetostructural studies carried out on analogous Fe^{III} and Fe₂^{III}Ni^{II} complexes [4,5].

4. Conclusion

In this study we employed high-field/frequency single-crystal and powder EPR techniques to study a low-spin Fe^{III} mononuclear building block which was subsequently used to synthesize a trinu-

clear $Fe_2^{III}Ni^{II}$ complex. Ferromagnetic exchange between the s=1/2 Fe^{III} monomers and the central Ni^{II} ion yields an interesting S=2 system that exhibits easy-axis type magnetic anisotropy. In future studies we plan to examine other members of this family and determine how the linearity of the bridging CN ligands, and steric effects dictated by ancillary ligands, affect the magnetic properties of the Fe_2^{III} building blocks and the nature of the magnetic exchange in the Fe_2^{III} Ni^{II} trinuclear clusters.

Acknowledgments

This work was funded by the National Science Foundation CHE0924374. C.B. would also like to acknowledge the NHMFL/FSU Shuler Fellowship. This work was performed at the National High Magnetic Field Laboratory, which is supported by the NSF (DMR1157490) and the State of Florida. S.M.H. gratefully acknowledges the National Science Foundation (Grant CHE 0914935, CAREER; Grant CHE 0939987) and the University of Missouri—St. Louis for financial support.

References

- [1] A. Panja, P. Guionneau, I.-R. Jeon, S.M. Holmes, R. Clérac, C. Mathonière, Inorg. Chem. 51 (2012) 12350.
- [2] I.-R. Jeon, R. Clerac, Dalton Trans. 41 (2012) 9569.
- [3] S.M. Taylor, G. Karotsis, R.D. McIntosh, S. Kennedy, S.J. Teat, C.M. Beavers, W. Wernsdorfer, S. Piligkos, S.J. Dalgarno, E.K. Brechin, J. Eur. Chem. 17 (2011) 7521.
- [4] Y.-Z. Zhang, U.P. Mallik, N.P. Rath, R. Clérac, S.M. Holmes, Inorg. Chem. 50 (2011) 10537.
- [5] Y.-Z. Zhang, U.P. Mallik, R. Clerac, N.-P. Rath, S.M. Holmes, Chem. Commun. 47 (2011) 7194.
- [6] J. Zarembowitch, O. Kahn, Inorg. Chem. 23 (1984) 589.
- [7] H. Oshio, K. Kitazaki, J. Mishiro, N. Kato, Y. Maeda, Y. Takashima, Dalton Trans. (1987) 1341.
- [8] D. Li, C. Ruschman, S. Parkin, R. Clerac, S.M. Holmes, Chem. Commun. (2006) 4036.
- [9] Y.-Z. Zhang, B.-W. Wang, O. Sato, S. Gao, Chem. Commun. 46 (2010) 6959.
- [10] A.K. Hassan, L.A. Pardi, J. Krzystek, A. Sienkiewicz, P. Goy, M. Rohrer, L.C. Brunel, J. Magn. Reson. 142 (2) (2000) 300.
- [11] M. Mola, S. Hill, P. Goy, M. Gross, Rev. Sci. Instrum. 71 (2000) 186.
- [12] S. Takahashi, S. Hill, Rev. Sci. Instrum. 76 (2005) 023114.
- [13] J. Lawrence, E.C. Yang, D.N. Hendrickson, S. Hill, Phys. Chem. Chem. Phys. 11 (2009) 6743.
- [14] S. Hill, S. Datta, J. Liu, R. Inglis, C.J. Milios, P.L. Feng, J.J. Henderson, E. del Barco, E.K. Brechin, D.N. Hendrickson, Dalton Trans. 39 (2010) 4693.